Journal of Applied Research and Technology
ISSN: 1665-6423
jart@aleph.cinstrum.unam.mx
Centro de Ciencias Aplicadas y Desarrollo Tecnológico
México

Lin, S. L.; Chang, H. C.; Huang, C. Y.
The Effect of Added Dead Space on Optimal Neuro-Muscular Drive and Respiratory Signals under Hypercapnia
Journal of Applied Research and Technology, vol. 12, núm. 6, diciembre, 2014, pp. 1003-1013
Centro de Ciencias Aplicadas y Desarrollo Tecnológico
Distrito Federal, México

The Effect of Added Dead Space on Optimal Neuro-Muscular Drive and Respiratory Signals under Hypercapnia

S. L. Lin*[1], H. C. Chang[2] and C. Y. Huang[3]

[1,2] Department of Automatic Control Engineering
Feng Chia University
Taichung, Taiwan, R.O.C.
[3] Office of Physical Education
Feng Chia University
Taichung, Taiwan, R.O.C.
*sllin@fcu.edu.tw

ABSTRACT
The problem concerning the nature and the function of the dead space is of basic importance for the full comprehension of the respiratory physiology and pathophysiology. To study the effect of an imposed external dead space on the optimal respiratory control system, we simulated the optimal neuro-muscular drive and respiratory signals, including instantaneous airflow and lung volume profiles, with dead space loading under hypercapnia. The dead space measurement model by Gray was employed and the human respiratory control simulator based on an optimality hypothesis was implemented. The ventilatory control simulations were performed with external dead space loading of 0, 0.4 and 0.8 liters under rest condition (P_{ICO_2}=0%) and CO_2 inhalation of 3% to 7%. The optimization of the respiratory signals and model behavior of the optimal respiratory control under dead space loading and hypercapnia were verified and found to be in general agreement with experimental findings.

Keywords: Dead space, respiratory control, neuro-muscular drive, respiratory signal, hypercapnia.

1. Introduction

Extended studies on the concept of dead space have been made in the last half-century. The problem concerning the nature and the function of dead space is of basic importance for the full comprehension of the respiratory physiology and pathophysiology [1-6]. Bohr used a mass balance method to measure dead space through the information of tidal volume, mixed alveolar gas, and expired alveolar gas compositions. Klocke [7] acknowledged that dead space values were important in the past, because alveolar ventilation was calculated from total ventilation using an assumed or empirical value for dead space. Fowler [8] determined dead space volume using Bohr's formula, with the conclusion that the regional non-uniformity of ventilation and lung volume were the most important factors in determining the dead space volume. Pappenheimer [9] proposed a new technique that utilizes constant alveolar gas tensions for measuring V_D, P_{ACO_2} and P_{AO_2}, which provides a graphic solution of the Bohr formula. Although it appeared a better method than Coon [10], Wolff [11] have described latter because of its independence of metabolic rate, however, the method depended on constancy of V_D. Maruyama [12] studied ventilatory response during external dead space breathing and CO_2 inhalation for given increase in P_{ETCO_2} with different levels of P_{ETO_2} (hyperoxia, normoxia, and hypoxia) in human. Lofaso [13] investigated the effect of positive or negative inspiratory pressure on respiration under external dead space loading. Poon [14] examined the effects of airway CO_2 loading on the response of ventilation-CO_2 output during exercise with and without external dead space.

The optimization and simulation techniques and tools have been well developed during the past decades and been widely applied in the field of engineering design [15,16] and biomedical research [17-20]. An earlier research by Poon [21] suggested that the ventilatory responses to CO_2 inhalation and exercise and can be predicted by the minimum criteria of a controller objective function including chemical and mechanical costs of breathing. It was later extended to model the

integrative control of $\dot{V}_E$ and respiratory pattern, by expressing the breathing work rate in terms of the respiratory neural drive P(t) [22]. The simulator implemented by Lin [17] constructed was based on the optimal respiratory control model with LabVIEW. Subject to any change in ventilation, we may observe the respiratory response and monitor the effect of the imposed experiments on wave shapes to various chemical stimuli in real-time.

An earlier study [18] was aimed to simulate and compare the effect of external dead space (EDS) loading on the ventilatory response of two distinct dead space measurement models, derived from Gray and Coon. Predicted behaviors with corresponding ventilatory responses were investigated and compared with experimental findings. While both dead space models produced satisfactory predictions on optimized $\dot{V}_E$ vs. P_{ACO2}, $\dot{V}_A$ vs. P_{ACO2}, F vs. P_{ICO2}, V_T vs. P_{ICO2}, $V_{D\text{-total}}$ vs. V_T, $V_{D\text{-total}}/V_T$ vs. V_T, $\dot{V}_E$ vs. V_T and $\dot{V}_A$ vs. V_T relationships, Gray's model provided better correlation and more consistent results throughout most of the ventilatory responses.

2. Method

Previous researches [17,18] have successfully proposed and implemented a simulation strategy based upon a mathematical model of the optimal respiratory control with MATLAB and LabVIEW. In current study, simulations were based upon the mathematical modeling of the optimal respiratory control, as illustrated in Fig. 1, with LabVIEW platform. The controller of the optimal chemical-mechanical respiratory control model of Fig. 1 is driven by both chemical and neuro-mechanical feedback signals. Figure 1 shows the coupling of chemical cost and mechanical cost. The fundamental hypothesis of the model is that a total cost function can be formulated to reflect the balance of a combined challenge (J) due to the chemical (J_C) and mechanical cost (J_M) of breathing [10]. The respiratory control feedback system is modeled with four major functional blocks: the plant, the feedback path, the controller, and the effector. The mathematical descriptions of four functional blocks have been detailed in earlier researches [17] and are outlined briefly below:

Gas Exchanger: The plant describes the events of the pulmonary exchange subject to the control signal $\dot{V}_E$(total ventilation in one minute, l/min) and disturbances in the inhaled and metabolic CO_2 and O_2 (P_{ICO2}/P_{IO2}, Torr, $\dot{V}_{CO_2}/\dot{V}_{O_2}$, l/min), and lactic acidosis. The system's outputs are the pressures of arterial CO_2 and O_2 (P_{aCO2}/ P_{aO2}, Torr), and $[H^+]_a$ (arterial H-ion concentration, mole/l). Because the conditions of normoxia and normal acid base condition will be assumed in the paper, only the effects on P_{aCO2} will be considered. The gas exchanger equation describes the dependence of the arterial blood gas tension on the total ventilation and other disturbances are given as [10,11,13]:

$$P_{aCO_2} = P_{ICO_2} + \frac{863 \cdot \dot{V}_{CO_2}}{\dot{V}_E\left(1 - {V_D}/{V_T}\right)} \quad (1)$$

where $P_{aCO}{}^2$ is assumed to be identical to mean

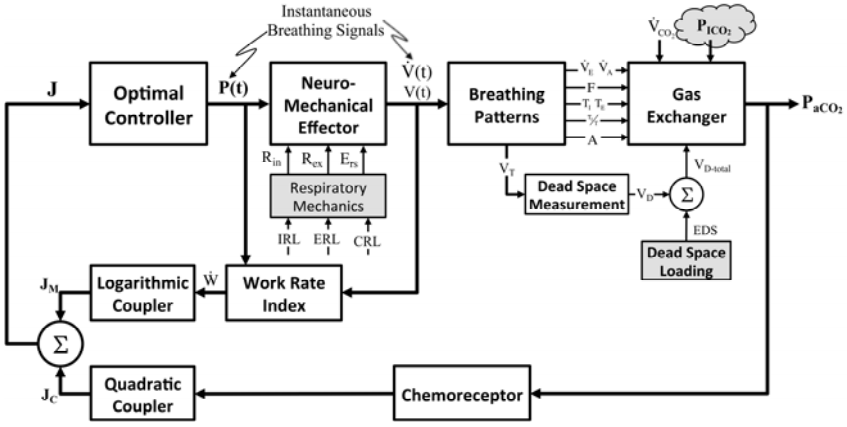

Figure 1. The mathematical modelling of the optimal chemical-mechanical respiratory control [17].

alveolar P_{CO}^2. Equation (1) describes the steady-state effect of ventilation on P_{aCO2} subject to any disturbances in the inhaled and metabolic production of CO_2.

Chemoreceptors: As depicted in Fig. 1, the feedback loop consists of two chemosensory structures, known as the central and peripheral chemoreceptors. The total chemical stimulation level of the controller (I_O, impulses/sec), the sum of the central (I_C, impulses/sec) and peripheral chemoreceptor stimulus (I_P, impulses/sec), can be expressed as a linear function of P_{aCO2} [17,23].

Neuro-Mechanical Effector: Instantaneous airflow is known to be controlled physiologically by neural impulses from the respiratory center (controller). The neuro-mechanical effector, which relates the neural respiratory output to the resultant mechanical airflow, is required for optimizing the neural input to the respiratory muscles to optimize the ventilatory airflow ($\dot{V}(t)$, L/min). The mechanical work of respiration results from the frictional resistance to airflow in the airways and the stretching of the elastic walls of the lungs and thorax. The neuro-mechanical effector can be described by the electrical analog of the linear or nonlinear model of respiratory mechanics, which characterizes the resistance of the airways, the lung inertance, and the compliance of the alveoli. To simplify the mechanical model of the respiratory system, the inertance was neglected when switching from the R-L-C model to the R-C model. In previous studies [17,18,21,22], we described the neuro-mechanical effector by using the electrical R-C model (Fig. 3(A)), based on a lumped-parameter model proposed by Younes and Riddle [24], for relating respiratory neural and mechanical outputs. In this model, the equation of motion is given by the following dynamic equation:

$$P(t) = \dot{V}(t) \cdot R_{rs} + V(t) \cdot E_{rs} \quad (2)$$

The parameters R_{rs} (cm-H_2O·l^{-1}·sec) and E_{rs} (=1/C_{rs}, cm-H_2O/l) represent the total flow-resistive and volume-elastic components, respectively, which include the passive resistances and elastance of the lung, chest wall, and airways. The waveshape of the neuro-muscular drive (P(t), cm-H_2O) is modeled into an inspiratory and expiratory phase. The inspiratory drive is approximated by a quadratic function and the expiratory pressure is represented by an exponential discharge function of the form (Fig. 2) [18,22]:

$$P(t) = a_0 + a_1 t + a_2 t^2 \quad 0 \le t \le t_1 \quad (3)$$

$$P(t) = P(t_1) \cdot e^{\frac{t-t_1}{\tau}} \quad t_1 \le t \le t_1 + t_2 \quad (4)$$

where the parameters a_0 and a_1 in Eq. (3) represent the net driving pressure and its rate of rise at the onset of the neural inspiratory phase, and the parameter a_2 describes the shape of the wave; t_1 (sec) and t_2 (sec) represent the neural inspiratory and expiratory duration, respectively. In Eq. (4), P(t_1) is the peak inspiratory pressure (cm-H_2O) and τ denotes the rate of decline of inspiratory activity.

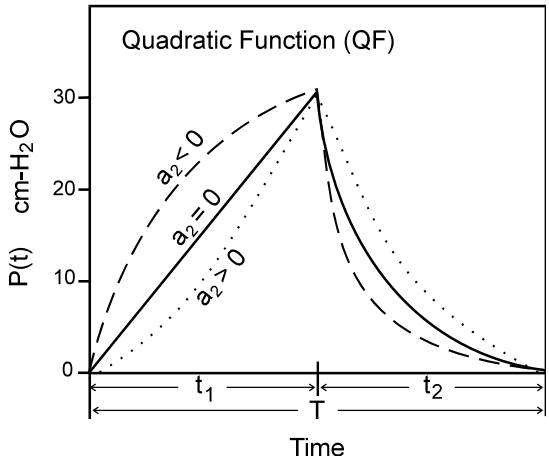

Figure 2. The waveshape of neural muscular drive over a complete respiratory cycle.

Optimal Controller. Poon [21,22] proposed and Lin [17,18] verified that an optimal controller might counterbalance the metabolic needs versus energetic needs of the body, and the resulting compromise would determine the ventilatory response. Rather than a reflex response to the chemical stimulus, the fundamental hypothesis of the optimal controller is that a total cost function (J) can be formulated to reflect the balance of a combined challenge due to chemical (J_C) and mechanical (J_M) cost of breathing [17,21,22]. The optimal control output is determined by the minimum of J, which consists of the square law for chemical feedback and logarithmic law for mechanical feedback,

conforming to Steven's law and Weber-Fechner law of sensory reception, respectively. On the other hand, the respiratory work rate $\dot{W}$, is assumed to be an explicit function of the respiratory neural drive and can be parameterized by the mechanical constraints of the respiratory system although this takes a quantitative description of the mechanical effector system.

Work Rate Index. Several mechanical indices have been previously studied for respiratory optimization [17, 21]. In the implemented simulator of current study, the mechanical work rate of inspiration and expiration are evaluated to predict the inspiratory waveshape and ventilatory responses to various types of system inputs.

$$\dot{W} = \dot{W}_I + \lambda \cdot \dot{W}_E \quad (5)$$

$$\dot{W}_I = \frac{1}{T}\int_0^{T_i} \frac{P(t)\cdot \dot{V}(t)}{\xi_1^n \cdot \xi_1^n} dt \quad (6)$$

$$\dot{W}_E = \frac{1}{T}\int_{T_i}^{T} P(t) \cdot \dot{V}(t) dt \quad (7)$$

In Eq. (5), the total mechanical index is assumed to be a weighted sum of the inspiratory and expiratory indexes with a weighting parameter λ, and $\dot{W}$, $\dot{W}_I$, and $\dot{W}_E$represent the total respiratory, inspiratory, and expiratory work rate (kg·m/sec), respectively [17]. The efficiency factors ξ_1 and ξ_2 of Eq. (7) account for the effects of the respiratory-mechanical limitation and the reduction in the neuro-mechanical efficiency with increasing effort. The overall efficiency is dependent on two factors: the maximal (P_{max}) and the maximum rising rate of neuro-muscular drive ($\dot{P}_{max}$).

Dead Space Modeling. When $\dot{V}_A$ was defined as the miniute volume of gas that, when in CO_2 equilibrium with arterial blood, must be expired to maintain $\dot{V}_{CO_2}$. Thus $\dot{V}_A$ is equal to the minute volume of gas expired from alveolar structures only when all these structures have a mean P_{aCO2} value equal to P_{aCO2}. Defining $\dot{V}_A$ in terms of $\dot{V}_{CO_2}$, then dead-space ventilation ($\dot{V}_D$) is defined as [25].

$$\dot{V}_E = \dot{V}_A + \dot{V}_D \quad (8)$$

The Eq. (8) can further be developed, firstly by Bohr, to measure the physiological dead space.

$$V_D = \frac{(F_{ACO_2} - F_{ECO_2})\cdot V_T}{F_{ACO_2}} \quad (9)$$

where F_{ACO2} is alveolar CO_2, F_{ECO2} is the fractional concentration of CO_2 from mixed expired gases.

$$V_D = \frac{(P_{ACO_2} - P_{eCO_2})\cdot V_T}{P_{ACO_2}} \quad (10)$$

The Bohr equation is considered to be complicated since it is based upon the fact that all CO_2 comes from alveolar gas and the exhalation of CO_2 can therefore be used to measure gas exchange or lack of gas exchange if there is alveolar dead space. For each tidal volume there will be a proportion of dead space (anatomical) but the amount of gas that is left over should take part in gas exchange.

Gray [25] proposed a dead space formulation that included the Bohr Formula, Washout equation and Virtual dead space equation. One of the original uses of the Bohr formula was to calculate alveolar composition from knowledge of the anatomical dead space and thus obviate the difficulties of alveolar sampling. Unfortunately the formula uses a “dead air” variable and not a space at all. Experiments also demonstrated the dependence of expired dead air volume on the tidal volume, particularly for the lower tidal volumes. In respiratory physiology the Bohr formula is applied to find many significant results. The washout equation is useful because in the washout phenomenon, the volume of the expired dead air must be a function of the expired tidal volume.

As a consequence of the washout phenomenon, the volume of expired dead air must be a function of the expired tidal volume. Rohrer suggested approximating this relationship by the physical law for the washing out of a rigid uniform cylinder by uniform laminar airflow.

$$DA = DS\left(1 - \frac{0.25\cdot DS}{TV}\right)$$
$$AA = TV\left(1 - \frac{0.5\cdot DS}{TV}\right)^2 \quad (11)$$

where DA represents the virtual dead air, AA represents virtual alveolar air, TV represents the volume of expiration flow, and DS represents the fixed volume of the cylinder. By rearrangement of the washout equation of Eq. (11) and combining it with the Bohr formula, Gray [25] obtained:

$$\mathrm{DS} = 2 \cdot \mathrm{TV}\left(1 - \sqrt{\frac{\mathrm{AA}}{\mathrm{TV}}}\right) = 2 \cdot \mathrm{TV}\left(1 - \sqrt{\frac{\mathrm{F_E} - \mathrm{F_I}}{\bar{\mathrm{F}}_\mathrm{A} - \mathrm{F_I}}}\right) \quad (12)$$

where F_I and F_E are the composition of inspired and expired air, respectively, and $\bar{F}_A$is the mean composition of the altered components in the virtual alveolar air.

Various reasons were given by Gray [25] for expecting the virtual dead space to increase with the inspiratory tidal volume. Gray firstly assumed that the virtual dead space could be approximated by a simple linear function [25]:

$$\mathrm{V_D} = \mathrm{V_{DS0}} + \mathrm{K_{DS}} \cdot \mathrm{V_T} \quad (13)$$

where V_{DS0} is the standard virtual dead space at zero tidal volume, K_{DS} is the increment in virtual dead space per unit increment in tidal volume. The empirical constants were obtained from experiments on five medical students by statistical fitting of the experimental data and permit evaluation of the fundamental variables V_{DS0} and K_{DS}. Based on the experimental results, the two dead space properties were effectively reduced by approximating K_{DS} as equal to $\frac{1}{8}$ of V_{DS0}, thus reducing Eq. (13) to

$$\begin{aligned}\mathrm{V_D} &= \mathrm{V_{DS0}} + 0.125 \cdot \mathrm{V_{DS0}} \cdot \mathrm{V_T} \\ &= \mathrm{V_{DS0}} \cdot \left(1 + \frac{\mathrm{V_T}}{8}\right)\end{aligned} \quad (14)$$

To account for the changes in anatomic dead space with airway caliber, Eq. (14) was employed with following empirical relation suggested [26]:

$$\mathrm{V_D} = 0.037 \cdot \mathrm{VC} \cdot \left(1 + \frac{\mathrm{V_T}}{8}\right) \quad (15)$$

where VC is vital capacity which ranging between 3 and 5 liters for normal adults.

3. Simulation Results and Discussion

The simulator's human-machine interface was constructed with a multilayered structure from main panel for an expandable modular design using the LabVIEW platform. Figure 3 shows the human respiratory control simulator's main control panel. From the **MAIN** panel of Fig. 3, the user can initiate a simulation via the **INPUT** panel by entering respiratory parameters including $\dot{V}_{CO_2}$ (metabolic rate of CO_2), P_{ICO_2} (partial pressure of inhaled CO_2), R_{in} (inspiratory airway resistance), R_{ex} (expiratory airway resistance), E_{rs} (lung elastance), and EDS (external dead space loading).

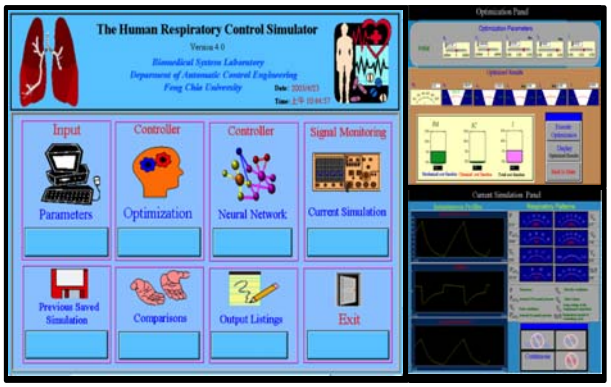

Figure 3. Main panel (left), optimization panel (upper right), and signal monitoring window for current simulation (lower right) in the simulator [17].

User selects controller from alternatives, **OPTIMIZATION** to optimize the respiratory waveforms and breathing pattern, or **NEURAL NETWORK** to use both the back-propagation neural network and forward model to obtain simulated results without going through the time-consuming optimization process. Selecting the **OPTIMIZATION** control opens the window shown on the upper right of Fig. 3. In the upper part of the window, the user is requested to define the initial parameters essential to the optimization. Once all of the initial estimates are entered, the user selects the "Execute Optimization" control. The optimization runs until the numerical calculation is completed and an optimum is reached. Clicking the "Display optimized results" control displays the optimized variables a_0, a_1, a_2, t_1, t_2, and τ in the center of the window. The obtained optimized parameters can then be used to compose the isometric pressure profile with Eq. (3) and Eq. (4). The simulation results can be observed through the **SIGNAL MONITORING OF CURRENT SIMULATION** panel, as shown in the lower right of Fig. 3. The "Instantaneous Profiles" windows demonstrate

three respiratory waveforms to be monitored: neuromuscular driving Pressure P(t), airflow $\dot{V}(t)$, and lung volume V(t). The respiratory patterns, including f, P_{aCO2}, V_T, P_{aO2}, $\dot{V}_{CO_2}$, $\dot{V}_{O_2}$, V_O, T_I, T_E, and T_I/T, are shown through the use of virtual instruments of LabVIEW and located in the upper right of the panel.

The resultant waveforms were simulated and monitored at varying levels of CO_2 inhalation and exercise in earlier study [17] without external dead space loading. As shown in Fig. 4, the instantaneous neuro-muscular driving pressure P(t), airflow rate $\dot{V}(t)$, and volume V(t), from top to bottom, respectively, are summarized at various levels of exercise CO_2 output ($\dot{V}_{CO_2}$=0.2, 0.6, 1.0) and inhaled CO_2 (P_{ICO_2}=2%, 3%, 5%, 7%). The simulator is built to be a useful platform as the model behavior of respiratory control can be investigated by examining the instantaneous responses of the waveforms under various breathing situations.

The results of current study were tabulated in Table 1 and Table 2. In Table 1, the optimized results of the optimization variables a_0, a_1, a_2, t_1, t_2, and τ under simulated EDS and P_{ICO2} levels were presented. By applying the Eqs. (3) and (4) with the optimized results of Table 1, the optimized neuro-muscular driving pressure profiles can be figured in the form of Fig. 4. On the other hand, with the use of the dynamic equation of Eq. (2) and proper mathematical operations [17,22], the optimized instantaneous airflow and lung volume profiles can also be derived. The tidal volume was obtained from lung volume profile ($V_T=V(t_1)-V(t_1+t_2)$) , and all the resultant breathing patterns, including P_{aCO2}, f, T_{TOT}, V_D, $\dot{V}_E$, and $\dot{V}_A$, were consequently derived as revealed in Table 2.

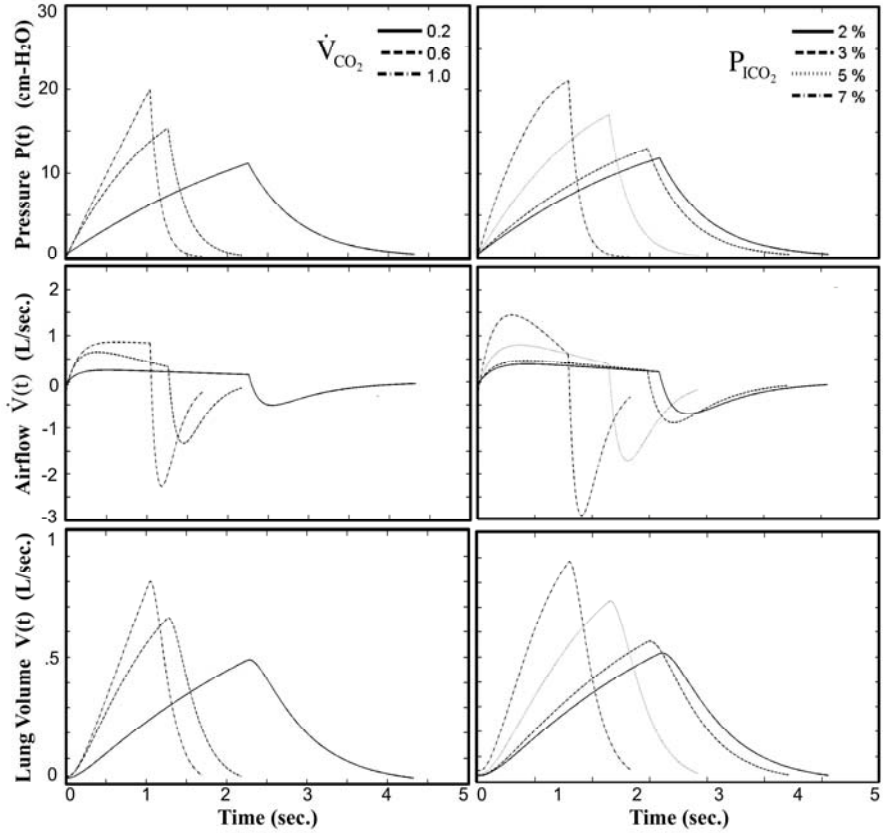

Figure 4. The optimized neuro-muscular driving pressure (P(t), top), airflow rate ($\dot{V}(t)$, middle), and lung volume (V(t), bottom) over a complete breathing cycle at various levels of exercise CO_2 output (left) and inhaled CO_2 (right) without external dead space loading.

EDS (l)	P_{ICO2} (%)	a_0 (cm-H_2O)	a_1 (cm-H_2O/min)	a_2 (cm-H_2O/min^2)	t_1 (min)	t_2 (min)	τ (min)
0	0	0.7750	435.457	-2202.630	0.0317	0.0467	0.0169
	3	0.3956	559.201	-2763.124	0.0286	0.0216	0.0060
	5	0.1328	1121.469	-6436.847	0.0163	0.0123	0.0025
	7	0.0722	2137.492	-44876.585	0.0183	0.0100	0.0017
0.4	0	0.3209	571.833	-2555.3801	0.0554	0.0570	0.0132
	3	0.3433	852.493	-5312.8530	0.0450	0.0301	0.0068
	5	0.6274	1452.570	-7997.1897	0.0281	0.0230	0.0057
	7	0.0506	2175.755	-24752.8000	0.0289	0.0116	0.0017
0.8	0	0.2088	790.231	-1795.5094	0.0500	0.0776	0.0151
	3	0.2874	942.913	-3104.1852	0.0495	0.0345	0.0070
	5	0.1605	934.184	2036.4325	0.0485	0.0212	0.0037
	7	0.1778	3181.404	-37015.1317	0.0235	0.0160	0.0028

Table 1. Results of the optimized parameters for neuro-muscular drive under added EDS and CO_2 inhalation.

EDS (l)	P_{ICO_2} (%)	P_{aCO_2} (Torr)	V_T (l)	f (bpm)	T_{TOT} (min)	V_D (l)	$\dot{V}_E$ (l/min)	$\dot{V}_A$ (l/min)
0	0	40.264	0.4913	12.75	0.0784	0.1551	6.2649	4.2867
	3	42.807	0.5728	19.93	0.0501	0.1566	11.4166	8.2953
	5	48.310	0.6362	34.99	0.0286	0.1578	22.2613	16.7406
	7	58.953	0.9821	35.44	0.0282	0.1641	34.8076	28.9916
0.4	0	39.743	1.0537	8.89	0.1124	0.1654	9.3719	4.3429
	3	42.177	1.2104	13.32	0.0751	0.1683	16.1241	8.5541
	5	48.082	1.4486	19.54	0.0512	0.1726	28.3096	17.1190
	7	58.741	1.7984	24.65	0.0406	0.1790	44.3373	30.0630
0.8	0	39.489	1.5320	7.84	0.1276	0.1741	12.0034	4.3709
	3	41.810	1.7093	11.90	0.0840	0.1774	20.3470	8.7128
	5	48.253	2.1585	14.35	0.0697	0.1856	30.9789	16.8340
	7	58.266	2.2834	25.30	0.0395	0.1879	57.7676	32.7753

Table 2. Results of the optimized breathing patterns under added EDS and CO_2 inhalation.

To examine the effect of an imposed dead space loading on the optimized instantaneous respiratory waveforms under different levels of CO_2 inhalation, Fig. 5 depicts the profiles with EDS=0, 0.4, and 0.8 l. As an EDS of 0.4 (l) was imposed and P_{ICO_2}=0% (left column of Fig. 5), in comparison with EDS=0, the optimized neuro-muscular drive P(t) (top row of Fig. 5) attains a higher amplitude with prolonged inspiratory duration (t_1) and higher duty cycle (T_I/T). As P_{ICO_2} was increased to 3% (middle column of Fig. 5) and 7% (right column of Fig. 5), the change of the waveshapes in P(t) displayed little difference with that of 0% but with higher magnitude. However, as an EDS of 0.8 (l) was imposed, we found that inspiratory duration and duty cycle were reduced to be less than those of EDS=0.4 (l) under the cases of P_{ICO_2}=0% and 7%.

The airflow profiles (middle row of Fig. 5) do not show substantial change in shape although the peak inspiratory and expiratory flow achieved higher rates with increased EDS loading or higher CO_2 inhalation level. The lung volume profiles also appear insignificant difference in shape but higher peak volumes with increased EDS

Figure 6 shows the effect of increased concentration of CO_2 inhalation on the optimized respiratory waveforms under three imposed EDS loading levels (EDS=0, 0.4, and 0.8 l). Without dead space loading (EDS=0), the waveforms of P(t) (top row of Fig. 5) are shaped as higher in rising rate (larger in a_1) and more concave upward (more negative in a_2) with increased P_{ICO2}. The effect of increase P_{ICO2} on inspiratory

duration and duty cycle is not as significant as on the increasing breathing frequency (decreasing period). As the imposed EDS was increased to 0.4 (middle column of Fig. 6) and 0.8 liters (right column of Fig. 6), the rising rates in P(t) become steeper as the concavities of the waveshape seem lesser. On the other hand, based on the airflow profiles on Fig. 6 (middle row), we also find that the increased P_{ICO2} level had shaped the $\dot{V}(t)$ from a rectangular-like waveform to a decending-like waveform with higher inspiratory and expiratory peak flows. As the EDS were increased to either 0.4 or 0.8 liters, the increasing in peak flow rate and the waveshaping in the inspiratory phase became more significant.

In Fig. 7, the effect of EDS loading (EDS=0, 0.4, and 0.8 l) on the optimized breathing patterns under various levels of CO_2 inhalation (P_{ICO2}=3%, 5%, and 7%), which were depicted in Table 2, are further summarized based on their percentage changes from rest condition (P_{ICO2}=0%). The hypercapnic response in P_{ICO2} (upper left of Fig. 7) seems to be unaffected among three levels of EDS loadings. At P_{ICO2}=3%, the increased EDS loading appears to have little effect on the variation in tidal volume (V_T, upper right of Fig. 7). However, the changes in V_T slightly increased (form 29.49% to 40.89%) at P_{ICO2}=5%, and significantly decreased (from 99.9% to 49.05%) at P_{ICO2}=7%, with elevated level of EDS loadings. The ventilatory response on tidal volume (V_T) should always be considered together with breathing frequency (f) for the attained total ventilation level ($\dot{V}_E=V_T \times f$) under any chemical or exercise stimuli. An opposite effect to the variation in tidal volume can be observed in breathing frequency as EDS loading was imposed during CO_2 inhalation, as was depicted in middle left of Fig. 7. Under different level of EDS, the changes in f are found to be nearly the same (≅50%) at P_{ICO2}=3%, and display a significant decreasing (from 174.43% to 83.04%) and slight increasing (from 177.96% to 222.70%) at P_{ICO2}=5% and 7%, respectively. As a result, we attain a minute ventilation level at marginally decreasing fashion with increasing EDS loading under each P_{ICO2} level, as was depicted in lower left of Fig. 7. Meanwhile, the resultant variations in alveolar ventilation $\dot{V}_A$(lower right of Fig. 7) are considerably stable in comparisons with the other breathing patterns at each CO_2 inhalation level.

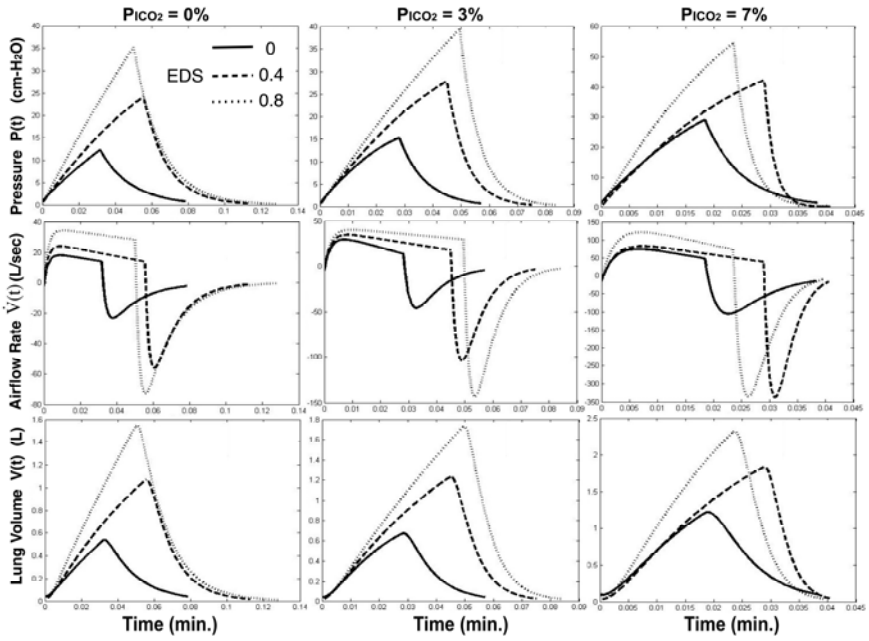

Figure 5. Effect of added EDS (0~0.8 l) on optimized waveshapes of P(t) (top), $\dot{V}(t)$ (middle), and V(t) (bottom) under P_{ICO2}= 0% (left), 3% (middle), and 7% (right).

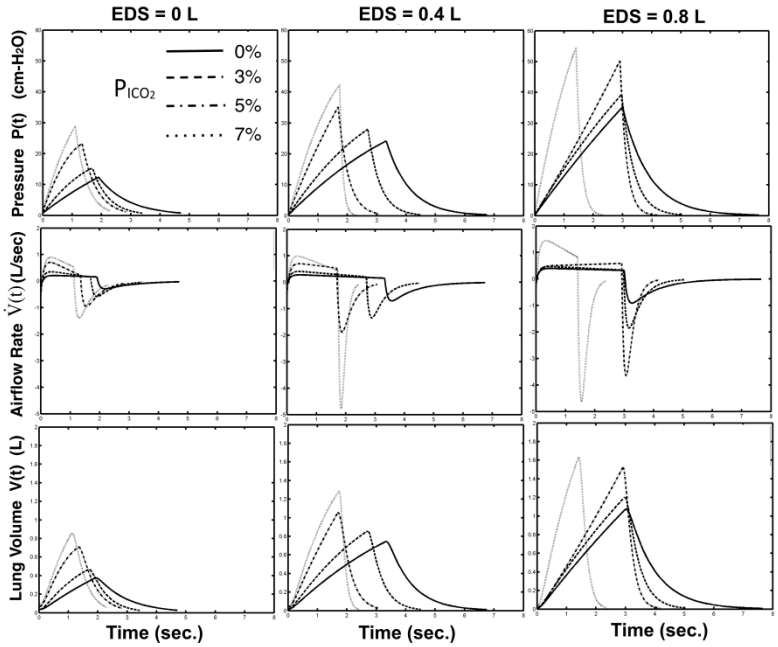

Figure 6. Effect of CO_2 inhalation (P_{ICO_2}= 0%, 3%, 5%, 7%) on waveshapes of P(t) (top), $\dot{V}(t)$ (middle), and V(t) (bottom) under EDS= 0 (left), 0.4 (middle), and 0.8 liters (right).

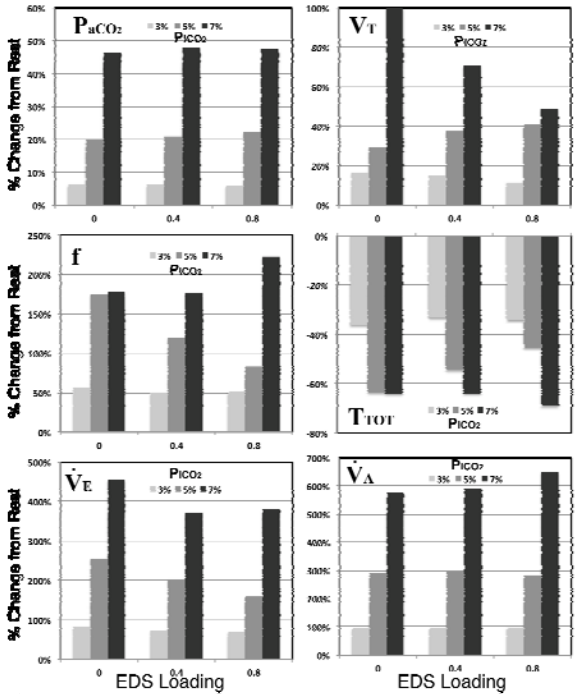

Figure 7. The percentage changes of breathing patterns from rest condition (P_{ICO_2}= 0%) with EDS loading at 0, 0.4, and 0.8 (l) under different levels of CO_2 inhalation (P_{ICO_2}= 3%, 5%, 7%). Left (from top to bottom): P_{ICO_2}, f, and $\dot{V}_E$; Right(from top to bottom): V_T, T_{TOT}, and $\dot{V}_A$.

4. Conclusions

With the use of the optimal respiratory control, a unified prediction of exercise and chemical responses was shown entirely in terms of conventional feedback-mechanisms instead of a separate stimulus signal, which has never been clearly demonstrated. With this model, a human respiratory control simulator is constructed to simulate the ventilatory responses under muscular exercise and CO_2 inhalation. We have examined the effects of external dead space loadings on the resultant ventilatory responses, including $\dot{V}_A$-P_{aCO_2}, $\dot{V}_E$-$\dot{V}_{CO_2}$, $\dot{V}_A$-$\dot{V}_{CO_2}$, F-$\dot{V}_{CO_2}$, V_T-$\dot{V}_{CO_2}$, and V_T-P_{aCO2} relationship, in earlier studies [17] for the simulations with different levels of EDS. Current study is aimed to explore the effect of the imposed dead space loading on the optimized respiratory profiles of pressure, airflow, and lung volume under increased levels of CO_2 inhalation. The simulation results show that higher amplitude with prolonged inspiratory duration and higher duty cycle were attained as EDS=0.4 (l) was imposed. The increase of EDS =0.8 (l) showed opposite effects on the inspiratory duration and duty cycle under P_{ICO2}=0% and 7%. No significant change in the waveshapes of these respiratory profiles was found with the imposed dead space loading under CO_2 inhalation. Current study attained valuable results in simulations of imposed dead space on respiratory control with the optimal respiratory control model. Further work can be extended to include the effects of respiratory mechanical (resistive or elastic) loading along with EDS loading.

Acknowledgments

This study was supported by grants NSC 101-2221-E-035-005 from the National Science Council, Taiwan.

References

[1] D. E. O'Donnell et al., "Pathophysiology of dyspnea in chronic obstructive pulmonary disease: a roundtable," Proc. Am. Thorac. Soc., vol.4, pp. 145-168, 2006.

[2] D. Sajkov et al., "Management of dyspnea in advanced pulmonary arterial hypertension," Curr. Opin. Support Palliat. Care, vol. 4, pp. 76-84, 2010.

[3] D. Jensen et al., "Effects of dead space loading on neuro-muscular and neuro-ventilatory coupling of the respiratory system during exercise in healthy adults: Implications for dyspnea and exercise tolerance," Respi. Physio. & Neuro., vol. 179, no. 2-3, pp. 219-226, 2011.

[4] M. N. van der Plas et al., "Pulmonary endarterectomy improves dyspnea by the relief of dead space ventilation," Ann. Thorac. Surg., vol. 89, no. 2, pp. 347-352, 2010.

[5] H. E. Wood et al., "Short-term modulation of the exercise ventilatory response in young men," J. Appl. Physiol., vol. 104, no. 1, pp. 244-252, 2008.

[6] C. S. Poon, "The classic potentiation of exercise ventilatory response by increased dead space in humans is more than short-term modulation," J. Appl. Physiol., vol. 105, no. 1, pp. 390, 2008.

[7] R. A. Klocke, "Dead space: simplicity to complexity," J. Appl. Physiol., vol. 100, no. 1, pp. 1-2, 2006.

[8] W. S. Fowler, "Lung function studies. II. The respiratory dead space," Am. J. Appl. Physiol., vol. 154, no. 3, pp. 405-416, 1948.

[9] J. R. Pappenheimer et al., "New experimental methods for determination of effective alveolar gas composition and respiratory dead space, in the anesthetized dog and in man," J. Appl. Physiol., vol. 4, no. 11, pp. 855-867, 1952.

[10] R. L. Coon and J. P. Kampine, "Measurement of dead space ventilation using a pHa servo-controlled ventilator," J. Appl. Physiol., vol. 51, no. 1, pp. 154-159, 1981.

[11] C. B. Wolff and R. C. Garratt, "Measurement of dead space ventilation," J. Appl. Physiol., vol. 53, no. 1, pp. 297-298, 1982.

[12] R. Maruyama, "Comparison of ventilatory response between dead space and CO2 breathing in humans," Jpn. J. Physiol., vol. 38, no. 3, pp. 321-328, 1988.

[13] F. Lofaso et al., "Respiratory response to positive and negative inspiratory pressure in human," Resp. Physiol., vol. 89, no. 1, pp. 75-88, 1992.

[14] C. S. Poon, "Potentiation of exercise ventilatory response by airway CO2 and dead space loading," J. Appl. Physiol., vol. 73, no. 2, pp. 591-595, 1992.

[15] M. Fathollah et al., "Developing a Conceptual Framework for Simulation Analysis in a Supply Chain Based on Common Platform," J. Appl. Res. Technol., vol. 7, no. 2, pp. 163-184, 2009.

[16] A. Huerta-Barrientos et al., "Optimizing the Cellular Network Planning Process for In-Building Coverage using Simulation," J. Appl. Research Tech., vol. 11, no. 6, pp. 912-919, 2013.

[17] S. L. Lin et al., "Modelling and simulation of respiratory control with LabVIEW," J. Med. Biol. Eng., vol. 32, no. 1, pp. 51-60, 2012.

[18] S. L. Lin et al., "Optimal respiratory control simulation and comparative study of hypercapnic ventilatory responses to external dead space loading," J. Mech. Med. Biol., vol. 13, Oct., 2013.

[19] J. R. Mendoza-Vázquez et al., "Simulation of a parallel mechanical elbow with 3 DOF," J. Appl. Research Tech., vol. 7, no. 2, pp. 113-123, 2009.

[20] A. M. Hernandez et al., "Learning respiratory system function in BME studies by means of a virtual laboratory: RespiLab," IEEE Trans. on Educ., vol. 51, pp. 24-34, 2008.

[21] C. S. Poon, "Ventilatory control in hypercapnia and exercise: optimization hypothesis," J. Appl. Physiol., vol. 62, no. 6, pp. 2447-2459, 1987.

[22] C. S. Poon et al., "Optimization character of inspiratory neural drive," J. Appl. Physiol., vol. 72, no. 5, pp. 2005-2017, 1992.

[23] C. S. Poon et al., "Homeostasis of exercise hyperpnea and optimal sensorimotor integration: The internal model paradigm," Resp. Physiol. Neurobi., vol. 159, no. 1, pp. 1-13, 2007.

[24] M. Younes and W. Riddle, "A model for the relation between respiratory neural and mechanical outputs, I. Theory," J. Appl. Physiol., vol. 51, no. 4, pp. 963-977, 1981.

[25] J. S. Gray et al., "Alveolar and total ventilation and the dead space problem," J. Appl. Physiol., vol. 9, no. 3, pp. 307-320, 1956.

[26] N. R. Anthonisen and J. A. Fleetham, "Ventilation: Total, Alveolar, and Dead Space," in D. M. Pollock (eds), Handbook of Physiology: The Respiratory System Gas Exchange, Washington, Am. Physiol. Soc., 1987, pp. 113-129.